Structural characterization of as-deposited cesium iodide films studied by X-ray diffraction and transmission electron microscopy techniques

Triloki, P. Garg and, B. K. Singh*

High Energy Physics laboratory, Physics Department, Banaras Hindu University, Varanasi 221005 India

Abstract

In this work, Cesium iodide (CsI) thin films with different thickness were prepared by thermal evaporation technique. The particle size of these films were determined by using X-ray diffraction (XRD) as well as by transmission electron microscopy (TEM) techniques. Although these two methods provide similar particle size in the case of semitransparent CsI films (4 nm and 20 nm) with nano scale size, there are discrepancies between the particle size in the case of thicker CsI films (100 nm and 500 nm). It indicates that for larger film thickness, XRD profile fails to determine the particle size in comparison with TEM measurement. Other physical parameters such as strain, stress and deformation energy density values were also estimated precisely for the prominent XRD peaks of thicker CsI films in the range $2\theta = 20^0 - 80^0$ by using a modified Williamson-Hall analysis assuming uniform deformation model (UDM), uniform deformation stress model (UDSM) and uniform deformation energy density model (UDEDM). The root mean square lattice strain calculated from the interplanar spacing and the strain calculated through UDM and UDSM were also compared.

1. Introduction

Alkali halide materials are of technological importance due to their excellent electron-emitting properties in the ultraviolet (UV), vacuum ultraviolet (VUV), X-ray ultraviolet (XUV) and X-ray energy ranges. These materials are currently employed in vacuum and gas-based photon detectors [1, 2], detection of scintillation light [3], medical imaging [4], positron emission tomography [5] as well as a protective layer in visible-sensitive photon detectors [6]. Among alkali halide materials, CsI is the best choice owing to its high quantum efficiency and relatively high stability to ambient air and gas environment [7, 8]. CsI films are also used to enhance the field emission (FE) sources which have potential applications including display devices [9], X-ray tubes [10], charged particle accelerators [11] and high power microwave devices [12]. Shiffler et al [13] has reported a reduction in outgassing and improved emission uniformity after CsI coatings on carbon fibers. Even two orders of magnitude reduction in turn-on voltage was successfully achieved by means of CsI coating on carbon fiber-based FE devices by the same group [14]. Due to this importance, several evaporation techniques including thermal evaporation [15, 16], ion beam scattering [17], e-gun evaporation [18], spray pyrolysis [19], pulsed laser deposition techniques [20] are being used to study the various physical and chemical properties of Cesium iodide films. However it has been observed that the thermal evaporation is the best choice forming a stoichiometric Cs:I ratio as well as the highest absolute quantum efficiency (QE) compared to other preparation techniques [17-20]. Even with its enormous applications in a variety of fields discussed above, very few of the earlier studies in this field deal with the structure characterization of CsI films [21]. It is well known that X-ray diffraction (XRD) and transmission electron microscopy are two important techniques which may be used for the structure characterization.

The present paper accounts for the surface characterization of as-deposited CsI thin films of different thickness prepared by thermal evaporation technique. A comparative evaluation of the mean particle size of as deposited CsI thin films obtained from direct TEM measurement, as well as XRD measurement is reported. In addition, the strain associated with the as-deposited CsI films due to lattice deformation was estimated by a modified form of Williamson-Hall approach [22] namely

*Corresponding author
Email address: bksingh@bhu.ac.in (B. K. Singh)

UDM. The other modified models such as UDSM and UDEDM provide an idea of the strain-stress as well as strain-energy density relation. The strain associated with the anisotropic nature is compared with the strain estimated from the interplanar spacing.

2. Experimental Details

The experimental setup for CsI consists of a high vacuum evaporation chamber which includes an oil-free Pfeiffer-made pumping unit having a pumping speed of 500 liter/second turbo-molecular pump and a diaphragm pump. Base pressure of this vacuum chamber is of the order of 3×10^{-7} Torr. Small pieces of CsI crystal were placed in a Tantalum boat inside the chamber and carefully heated to allow out-gassing from the surface of the crystal, if any, under a shutter. After proper out-gassing and melting of CsI crystals, thin films of different thickness were deposited on polished Aluminum (Al) substrates and formvar coated copper grids. Before deposition, typical composition of different residual gases including water vapor inside the chamber was monitored through a residual gas analyzer (SRS RGA 300 unit) as shown in Fig. 1 and it was ensured that water vapor is under controlled manner. During the film deposition,

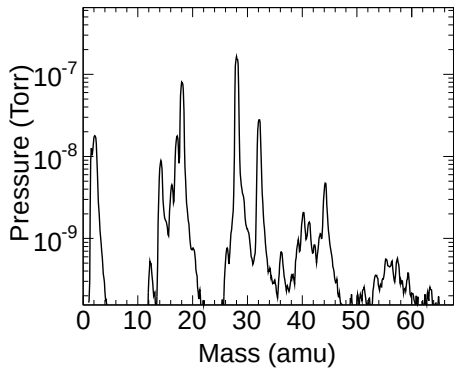

Figure 1: Residual gas composition inside the vacuum chamber.

the rate of evaporation was about 1-2 nm per second and the distance between the boat and substrate was kept a distance of about 20 cm. The thickness of the film was controlled by a quartz crystal thickness monitor (Sycon STM100).

After the film deposition, vacuum chamber was purged with nitrogen gas in order to avoid the effect of humidity on the prepared CsI samples. Immediately after the chamber opening under constant flow of nitrogen (N_2) gas, as-deposited CsI thin films were extracted and placed in a vacuum desiccator. Further, CsI films deposited on formvar coated copper (Cu) grid were introduced for TEM measurement while CsI films deposited on Al substrate for XRD measurement.

The structural measurements was performed by X-ray diffraction (XRD) measurement in the Bragg-Brentano parafocussing geometry on a PANalytical XPert PRO XRD system. The incident beam optics consisted of a CuK_α radiation source (λ = 1.5406Å), filtered with nickel (Ni) and operated at 40 kV and 30 mA. XRD measurements has been performed in continuous scan mode in the range $2\theta = 20^0 - 80^0$. The diffracted beam optics consists of a 0.04 rad soller slit and a scintillator detector. Similarly, transmission electron microscopy (TEM) was done by means of FEI Tecnai $20G^2$ operating at 200 KV voltage for the examination of structure and particle size of CsI films.

3. Results and discussion

3.1. Crystallite size and strain by XRD analysis

XRD patterns of cesium iodide thin films with different thickness prepared by thermal evaporation technique are shown in Fig. 2. No extra diffraction peaks

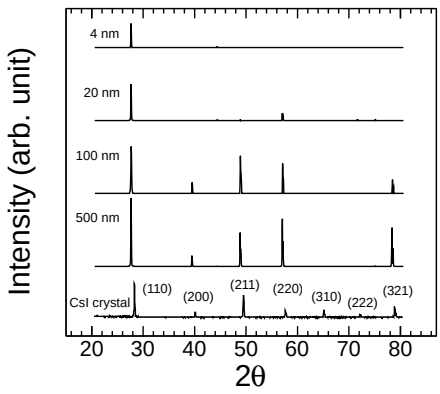

Figure 2: X-ray diffraction pattern of CsI thin films of different thickness, deposited on aluminum substrate and of CsI crystal.

corresponding to Cs, Cs_2O, $CsIO_3$ or other CsI phases are detected indicating that pure CsI is of polycrystalline, stoichiometric nature. Also XRD result of raw CsI crystal used for thermal evaporation is shown for

comparison (Fig. 2). The XRD scan exhibits a number of intense and sharp peaks which are assigned to the indicated Bragg reflections from CsI crystal. We may observe that the lattice plane corresponding to the preferred peaks for CsI crystal are: (110), (200), (211), (220), (310), (222) and (321). In the case of 4 nm as-deposited CsI thin films, we observe the peak of (110) lattice plane only. In the case of 20 nm as-deposited films, we observe the lattice plane corresponding to the peaks of (110) and (220) only. However for thicker as-deposited CsI films (100 nm and 500 nm), most intense peaks of (110) followed by (200), (211), (220) and (321) can be clearly observed. These peaks match with the peak positions listed for Cesium Iodide in ASTM card No. 060311 confirming the films to be that of CsI films. Using XRD profile shown in Fig. 2, lattice parameters of CsI crystal as well as CsI thin films were also calculated. The lattice constant values for all thicknesses of CsI film obtained is about $a = 4.666$Å, however lattice constant value for CsI crystal is about $a = 4.566$Å.

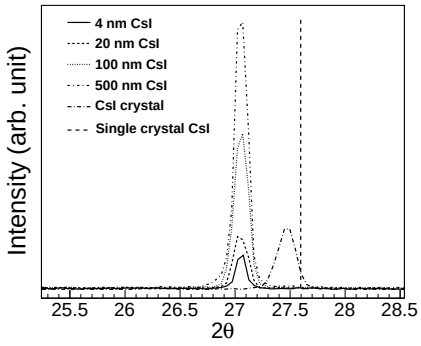

Figure 3: Shifts in the (110) peaks of the X-ray diffraction pattern as compare to single crystal shown with sharp line.

The average crystallite size was also calculated using Debye-Scherrer's equation [23],

$$D = \frac{k\lambda}{\beta_{hkl}\cos\theta} \tag{1}$$

Where D is the volume weighted crystallite size, k is the shape factor (0.89), λ is the wavelength of CuK_α radiation source, β_{hkl} is full width at half maxima (FWHM) of the particular peak and θ is the Bragg's angle. From the calculations, the average crystallite size of CsI thin films were obtained: 41 nm for 4 nm thin CsI film, 55 nm for 20 nm thin CsI film, 54.74 nm for 100 nm and 500 nm thick CsI films respectively. The crystallite size obtained by us is in good agreement with the reported crystallite size of 45 nm for 100 nm CsI thin films by Nitti et al [17] using same thermal evaporation technique. Klimonsky et al [19] have also reported the crystallite size of about 45-50 nm for different CsI samples prepared by spray pyrolysis technique. However for same thickness (100 nm) of CsI thin film deposited by means of ion beam sputtering and ion beam assisted sputtering techniques, Nitti et al [17] have reported the increased crystallite size of about 334 and 288 nm respectively indicating that the intensity of the Bragg peaks are quite narrow and sharp in nature. Williamson-Hall approach [22] allows us to separate two different reasons for a xrd peak broadening: one is the peak broadening from the crystallite size which varies as $1/\cos\theta$ (equation 1) and another is strain (ϵ) induced peak broadening which is given by Wilson formula ($\beta_{hkl} = 4\epsilon\tan\theta$) [24]. Here XRD data profile can also be used to determine residual stress in the sample. The apparent shift in diffraction peaks from their corresponding crystal data indicates a uniform stress originated in the film due to the thermal evaporation [26, 27]. A shift in the peak position of our CsI thin films of thickness from 4nm to 500 nm is also observed as shown in Fig. 3 for (110) plane, in comparison with the peaks observed in XRD scan of CsI crystals indicating that films are in a stressed state. In our case, CsI (110) peak is shifted towards lower angle which indicates that a tensile stress is acting on the as-deposited CsI films as compared to the crystal data ($2\theta = 27.592^0$) from ASTM card No. 060311 shown as a sharp line. Also one can see that CsI (110) peak for 4 nm to 500 nm thick films are shifted from the lower angle as compared to raw CsI crystal as shown in Fig. 2 and FIg. 3. These stresses acting in the film arise due to the various methods of film preparation and can cause some effects on the properties of the materials. The so called internal stress in the prepared film is calculated after the strain in it is calculated using Williamson-Hall relation [22]:

$$\beta_{hkl}\cos\theta = \frac{k\lambda}{D} + 4\epsilon\sin\theta \tag{2}$$

Where ϵ is strain, which is usually assumed to be proportional to the square root of the density of dislocations. A plot is drawn with the measured value of $\beta_{hkl}\cos\theta$ as a function of $4\sin\theta$ (see Fig. 4). One can achieve the strain from the slope of the fitted line and crystallite size (D) from its intersection with the y-axis. Equation (2) assumes that the strain is uniform in all crystallographic directions and known as uniform deformation model UDM). In this model description, it is assumed that the properties of material are independent of the direction along which it is measured. The UDM prediction for 100 nm and 500 nm thick CsI films are

Table 1: Geometric parameters of CsI thin films of different thickness

Williamson-Hall Method											
CsI Sample	Scherre's Method D (nm)	Uniform Deformation Model (UDM)		Uniform Deformation Stress Model (UDSM)			Uniform Deformation Energy Density Model (UDEDM)				TEM Particle Size (nm)
		D (nm)	Strain (ϵ) $\times$ 10^{-4}	D (nm)	Stress (σ) MPa	Strain (ϵ) $\times$ 10^{-4}	D (nm)	Energy Density (u) kJm^{-3}	Stress (σ) MPa	Strain (ϵ) $\times$ 10^{-4}	
500 nm	54.74	93.2	7.96	92.64	13.92	7.72	92.95	5.55	14.18	7.84	306
100 nm	54.74	93.5	7.76	92.95	13.56	7.52	93.26	5.27	13.82	7.64	303
20 nm	55.0										116
4 nm	41.0										42

shown in Fig. 4(a) and Fig. 4(d). From the plot, it is clear that the strain as well as the estimated crystallite size obtained for 100 nm and 500 nm thickness are the same (see Table 1 for details). It indicates that by adding more CsI layer does not produce any additional strain as well as any enhancement in crystallite size for 500 nm compared to 100 nm film. However it is unrealistic for a crystalline material such as CsI in our case. In this case, to consider anisotropic approach is more realistic. Therefore Williamson-Hall equation is modified by an anisotropic strain $\epsilon = \sigma/E_{hkl}$, where E_{hkl} is the Young's modulus in direction hkl and σ is the stress. In this approach, equation (2) is transformed into equation (3):

$$\beta_{hkl}\cos\theta = \frac{k\lambda}{D} + \frac{4\sigma\sin\theta}{E_{hkl}} \tag{3}$$

The reciprocal of Young's Modulus in the direction of the unit vector l_i in the cubic system is

$$\begin{aligned}\frac{1}{E_{hkl}} &= s_{11} - 2\left(s_{11} - s_{12} - \frac{1}{2}s_{44}\right)\left({l_1}^2{l_2}^2\right. \\ &+ \left.{l_2}^2{l_3}^2 + {l_3}^2{l_1}^2\right)\end{aligned} \tag{4}$$

Where s_{11}, s_{12} and s_{44} are the elastic compliances of CsI. Following relations provide the connection between the elastic compliances and the stiffness

$$c_{11} = \frac{(s_{11}+s_{12})}{(s_{11}-s_{12})(s_{11}+2s_{12})} \tag{5}$$

$$c_{12} = \frac{-s_{12}}{(s_{11}-s_{12})(s_{11}+2s_{12})} \tag{6}$$

$$c_{44} = \frac{1}{s_{44}} \tag{7}$$

where respective stiffness values are $2.434\times10^{11}d/cm^2$, $0.636\times10^{11}d/cm^2$ and $0.6316\times10^{11}d/cm^2$ respectively [25].

A plot is drawn with the measured value of $\beta\cos\theta$ as a function of $4\sin\theta/E_{hkl}$ as shown in Fig. 4(b) and Fig. 4(e) and uniform deformation stress σ was calculated from the slope of the line. The anisotropic lattice strain can also be calculated if E_{hkl} values for CsI films are known. Crystallite size can also be estimated from the intersection of y-axis as depicted in Table 1 for 100 nm and 500 nm CsI films respectively by means of uniform deformation stress model (UDSM). However it may be more reasonable to expect the real parameter for the deformation to be the deformation energy density (u). According to Hookes law, the deformed energy density u (deformed energy per unit volume) as a function of strain is $u = \epsilon^2 E_{hkl}/2$. Assuming this deformation energy density (u), equation (3) can be further modified in to the form:

$$\beta_{hkl}\cos\theta = \frac{K\lambda}{D} + 4\sin\theta\left(\frac{2u}{E_{hkl}}\right)^{1/2} \tag{8}$$

Uniform deformed energy density model (UDEDM) can be calculated from the slope of the line plotted between $\beta_{hkl}\cos\theta$ and $4\sin\theta(2/E_{hkl})^{1/2}$ as shown in Fig. 4(c) and Fig. 4(f). The strain can also be calculated by knowing the E_{hkl} values and shown in Table 1. Young's modulus (E_{hkl}) has been calculated and comes out to be of about 17.2873 GPa for (110) lattice plane followed by E_{hkl} = 21.7048 GPa for (200), E_{hkl} = 17.2873 GPa for

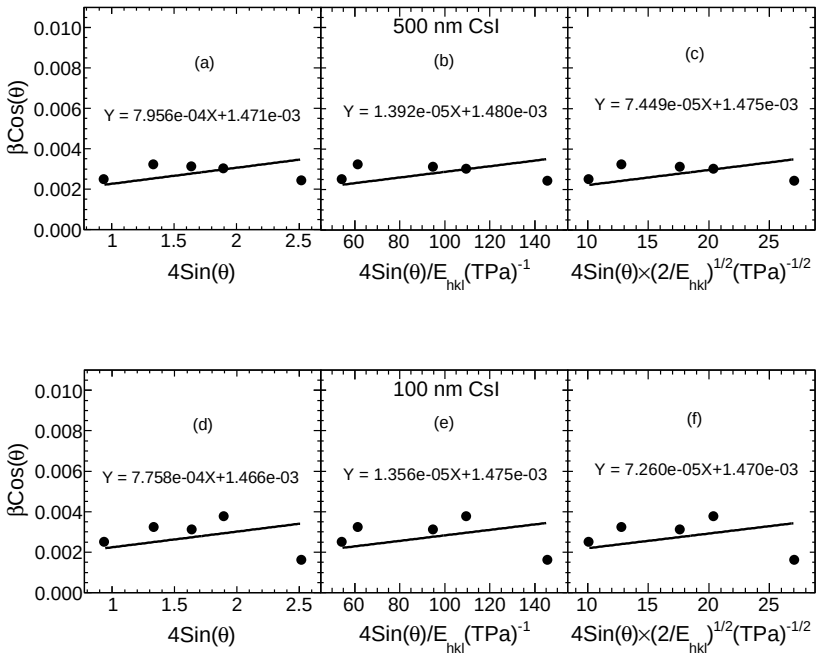

Figure 4: Williamson-Hall plots of 500 nm and 100 nm CsI film assuming (a,d) uniform deformation model (b,e) uniform deformation stress model and (c,f) uniform deformation energy density model.

(211), E_{hkl} = 17.2873 GPa for (220) and E_{hkl} = 17.2873 GPa for (321) lattice plane. Table 1 summarizes the geometrical parameter of CsI films of different thickness obtained from Debye-Scherrer's formula, various methods of W-H analysis and TEM measurement. By comparing the average value of crystallite size as well as the internal strain, stress obtained from the modified W-H analysis, it is evident that the different values are almost the same indicating the inclusion of strains in various form of W-H analysis has a very small impact on the average crystallite size of CsI films. However there is a very little variation between the crystallite size obtained from Debye-Scherrer's equation and the modified W-H analysis. This difference might be possible due to the difference in averaging the particle size distribution.

Fig. 4 shows the comparison of these three equations (Equation 2, 3 and 8) for 100 nm and 500 nm thick CsI films respectively. The deviation of data points away from the linear fit is less in the case of equation (8). Therefore one may assume that the uniform deformed energy density is found to be more appropriate/better for CsI samples.

To calculate the applied stress in a polycrystalline sample from XRD technique, it is necessary to consider only those particle which are properly oriented to diffract the incident X-ray beam. As a result the X-ray elastic constants connecting the RMS strain $\left(\epsilon_{RMS} = \sqrt{2/\pi} \times (\Delta d/d_{obs})\right)$ can be estimated and plotted against those estimated from the uniform deformation energy density method ϵ_{hkl} [28] as shown in Fig. 5. Here Δd is the difference between d_{obs} (observed in-

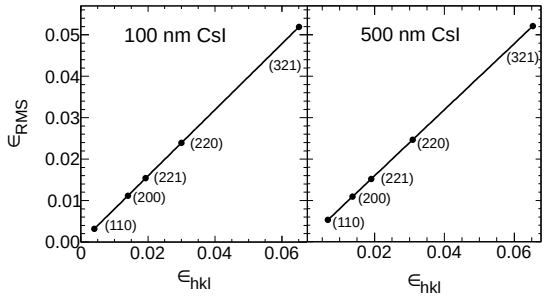

Figure 5: RMS lattice strain (ϵ_{RMS}) estimated from interplanar spacing plotted against lattice strain (ϵ_{hkl}) from uniform deformation energy density model (UDEDM)

terplanar spacing) and d_{ASTM} (single crystal interplanar spacing). In principle, if the strain estimated by means of the peak position as well as from the uniform deformation energy density method agrees, all the data points should lie on a straight line making an angle of 45^0 with the X-axis. This behaviour is more or less confirmed from the plot of RMS lattice strain (ϵ_{RMS}) as a function of the estimated strain calculated from the interplanar spacing. Hence one may observe that RMS strain varies linearly. However it is necessary to point out that the rms strain (ϵ_{RMS}) as well as the strain from UDEDM (ϵ_{hkl}) were estimated by completely different methods.

3.2. Particle size and diffraction pattern from TEM

TEM measurements are supposed to be a better tool for particle size determination due to the produced image of the sample. The result obtained from TEM analysis as shown in Fig. 6 shows that in the case of the 4 nm semi transparent CsI film, layer did not appear to be continuous exhibiting a surface coverage of 29% only. The average size estimated from TEM image is about 41 nm. Selected area electron diffraction (SAED) pattern of CsI films as shown in Fig. 7 (a) clearly shows that 4 nm CsI films are polycrystalline structure and do not have any impurities. This is in close agreement with the results obtained from XRD measurement (see Table 1) as well as the estimated value obtained from W-H analysis. In case of 20 nm films, layers exhibit morphology of interconnected crystallites of discontinuous structure; the average size was about 116 nm. For thicker films of 100 nm and 500 nm thickness layers exhibit quite uniform with larger particles compared to thinner CsI films. In this thick CsI films of 100 nm and 500 nm, particle have a columnar shape with a hexagonal shape having average size of about 300 nm. One may observe from Fig. 6 that the particle size and density is dependent on the film thickness. For semi-transparent CsI films, density of particle is very less and discontinuous in nature, However with increasing thicknesses, both particle size as well as the density is increased and film surface is fully covered.

Fig. 7 shows selected area electron diffraction patterns of CsI thin film of various thicknesses i.e. (a) 4 nm, (b) 20 nm, (c) 100 nm and (d) 500 nm. It has been observed that the SAED pattern obtained from CsI thin films of various thicknesses are crystalline in nature. The SAED pattern of 4 nm CsI thin film demonstrates that the film have randomly oriented particle. However SAED patterns obtained from 20 nm, 100 nm and 500 nm CsI thin films shows a discrete lattice of sharp spots which demonstrates that the film are of single crystal domain. The inter planar spacing and corresponding (hkl) crystallographic planes obtained from CsI thin film corresponds to a body centered cubic (bcc) structure with lattice constant $a = 4.666$Å. The experimental inter planar distances derived from the diffraction pattern between (hkl) crystallographic planes found to have a good match which is given in ASTM card No. 060311 with lattice constant $a = 4.566$Å.

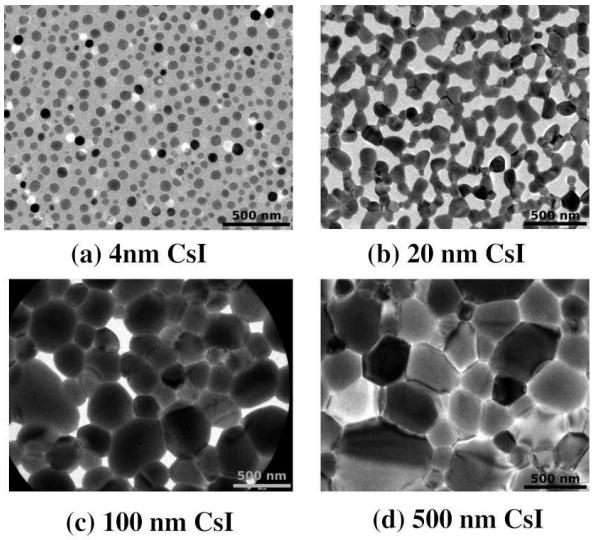

Figure 6: Transmission electron microscope (TEM) surface image of a) 4 nm, b) 20 nm, c) 100 nm and d) 500 nm as-deposited CsI thin films.

By comparing the results obtained from XRD and TEM analysis, there is good correlation between TEM and XRD measurements for semi transparent CsI films. However for the sample with increasing thickness, there is an apparent discrepancy between the particle sizes obtained by these two different methods in which particle size measured by TEM counting is higher than that from XRD analysis. When the thickness of film is increased from 20 nm to 500 nm, crystallite size obtained from XRD analysis remains constant however in case of TEM measurements, particle size increases sharply. It indicates that according to the results from XRD analysis, particle growth settles to be saturated around 20 nm and further adding more thickness does not boost the crystallite size. The results from TEM analysis contradicts it by revealing that the particle size of thicker films such as 100 nm and 500 nm is much higher than the value from XRD analysis (see Table 1).

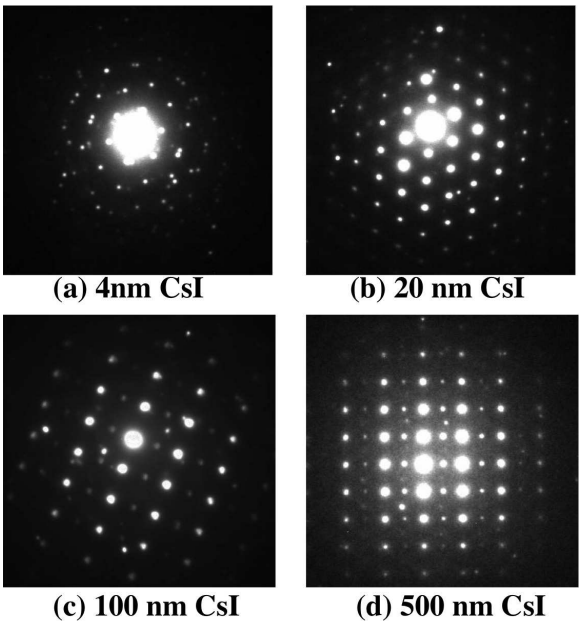

Figure 7: The electron diffraction pattern obtained from as-deposited CsI thin films of a) 4 nm, b) 20 nm, c) 100 nm and d) 500 nm thickness.

4. Conclusion

Thin and thick films of CsI were deposited by thermal evaporation technique and were characterized by XRD and TEM measurements in order to investigate the relationship between the two methods on structural characterization. Based on the results achieved, some conclusions can be drawn as below:

The displacement of (110) diffraction peaks towards the lower side from their corresponding crystal data indicates that tensile stress exists for all CsI samples.The line broadening of as-deposited CsI films due to small crystallite size was analysed by Debye-Scherrer's formula. A modified W-H method has been used to estimate the crystallite size, and strain induced broadening due to the lattice deformation with the amorphous nature. Estimated RMS strain are in agreement with the strain value calculated from difference in interplanar spacing. To the best of our knowledge, a detailed study using UDM, UDSM and UDEDM on the CsI films is not reported yet. We may suggest that these models can be precisely used for the estimation of the particle size of CsI films. In our case, all these models are found to be useful from the determination of crystal size.

Both XRD and TEM measurements show that the particle size for 4 nm and 20 nm thin films CsI are comparable. While for thicker films (100 nm and 500 nm), both XRD and TEM measurement provide different particle sizes; TEM provides with higher values of particle sizes in comparison with that of XRD analysis. It indicates that for the large grain sized materials, XRD analysis fails its usefulness for the particle size determination. However the particle size calculated from XRD data are qualitatively close to the that of particle size estimated from the modified W-H method.

5. Acknowledgment

This work was partially supported by the Department of science and technology (DST), the council of scientific and industrial research (CSIR) and by Indian Space Research Organization (ISRO), Govt. of India. Triloki acknowledges the financial support obtained from UGC under research fellowship scheme for meritorious students (RFSMS) program while P. Garg acknowledges the financial support from CSIR under senior research fellowship program.

References

[1] C. Lu and K.T. Mcdonald, Nuclear Instruments and Methods A 343 (1994) 135-151.
[2] D. Mormann et al., Nuclear Instruments and Methods A 478 (2002) 230-234.
[3] Daisuke Totsuka et al., Optical Materials 34 (2012) 1087-1091.
[4] Wei Zhao et al., Med. Phys. 31 (2004) 2594.
[5] F. Garibaldi et al., Nuclear Instruments and Methods A 525 (2004) 263-267.
[6] A. Breskin et al., App. Phys. Lett. 69 (1996) 1008.
[7] A. Breskin, Nuclear Instruments and Methods A 387 (1997) 1-18 (and references therein).
[8] A. Breskin, Nuclear Instruments and Methods A 367 (1995) 326-331 (and references therein).
[9] V. Vlashos et al., Vacuum Electron Conference 2009 IVEC, IEEE international, pages 333-334.
[10] Toru Hara et al., Rev. Sci. Instrum. 71 (2000) 3624.
[11] A. Jhingan and P. Sugathan., Proceeding of DAE Symposium on nuclear physics (2012) 463.
[12] R.J. Umstattd et al., Proc. of SPIE 3701 (1999) 8-13.
[13] D.A. Shiffler et al., IEEE Trans. Plasma Sci. 30, 1592 (2002) and references therein.
[14] D.A. Shiffler et al., J. App. Phys. 103, 013302 (2008).
[15] V. Dangendorf et al., Nuclear Instruments and Methods A 289 (1990) 322-324.
[16] J. Seguinot et al., Nuclear Instruments and Methods A 297 (1990) 133-147.
[17] M.A. Nitti et al., Appl. Phys. A 80, (2005) 1789-1791.
[18] P. Maier-Komor et al., Nuclear Instruments and Methods A 362 (1995) 183-188.
[19] S.O. Klimonsky et al., Inorganic materials, 2011 47 pp1033-1038.
[20] S.B. Fairchild et al., J. Vac. Sci. Technol. A 29 (2011) 031402.
[21] A.S Tremsin, S Ruvimov and O.H.W Siegmund., Nuclear Instruments and Methods A 447 (2000) 614-618.
[22] G. K.Williamson, W.H. Hall, Acta Metall. (1953) 1, 22.
[23] P. Scherrer, Gottinger Nachrichten (1918) 2, 98.

[24] A.R. Stokes, A.J.C. Wilson, Proc. Roy. Soc. London (1944) 56, 174.
[25] K. Reinitz, Physical Review 123 (1961), 1615-1619.
[26] G.C. Budakoti et al., Phys. Status Solidi A. 202 (2005) R7-R9.
[27] P. Arun et al., Journal of Physics and Chemistry of Solids. 71 (2010) 163-169.
[28] Dapiaggi, M, Geiger, CA, Artioli, G: Am. Miner. 90, 506 (2005)